CellPress

Structure
Article

# Telomeric Overhang Length Determines Structural Dynamics and Accessibility to Telomerase and ALT-Associated Proteins

Helen Hwang,[1,2] Alex Kreig,[1] Jacob Calvert,[1] Justin Lormand,[3] Yongho Kwon,[4] James M. Daley,[4] Patrick Sung,[4] Patricia L. Opresko,[3] and Sua Myong[1,5,6,*]

[1]Bioengineering Department, University of Illinois, 1304 West Springfield Avenue, Urbana, IL 61801, USA
[2]Medical Scholars Program, University of Illinois, 506 South Matthews Avenue, Urbana, IL 61801, USA
[3]Department of Environmental and Occupational Health, University of Pittsburgh, 100 Technology Drive, Suite 326, BRIDG, Pittsburgh, PA 15219, USA
[4]Department of Molecular Biophysics and Biochemistry, Yale University, 333 Cedar Street, P.O. Box 208024, New Haven, CT 06520, USA
[5]Institute for Genomic Biology, University of Illinois, 1206 West Gregory Street, Urbana, IL 61801, USA
[6]Physics Frontier Center (Center of Physics for Living Cells), University of Illinois, 1110 West Green Street, Urbana, IL 61801, USA
*Correspondence: smyong@illinois.edu
http://dx.doi.org/10.1016/j.str.2014.03.013

## SUMMARY

**The G-rich single-stranded DNA at the 3′ end of human telomeres can self-fold into G-quaduplex (GQ). However, telomere lengthening by telomerase or the recombination-based alternative lengthening of telomere (ALT) mechanism requires protein loading on the overhang. Using single-molecule fluorescence spectroscopy, we discovered that lengthening the telomeric overhang also increased the rate of dynamic exchanges between structural conformations. Overhangs with five to seven TTAGGG repeats, compared with four repeats, showed much greater dynamics and accessibility to telomerase binding and activity and loading of the ALT-associated proteins RAD51, WRN, and BLM. Although the eight repeats are highly dynamic, they can fold into two GQs, which limited protein accessibility. In contrast, the telomere-specific protein POT1 is unique in that it binds independently of repeat number. Our results suggest that the telomeric overhang length and dynamics may contribute to the regulation of telomere extension via telomerase action and the ALT mechanism.**

## INTRODUCTION

Human telomeres terminate in a 50–200-nucleotide single-stranded 3′ overhang that plays a pivotal role in chromosome end protection (Makarov et al., 1997; McElligott and Wellinger, 1997; Wright et al., 1997). The G-rich overhang serves as the substrate for telomerase that extends telomeres by adding tandem TTAGGG repeats (Greider and Blackburn, 1987) and as a binding site for the POT1 protein that prevents the activation of the checkpoint kinase ataxia telangiectasia and Rad3 related (ATR), inhibits sister chromatid fusion, and represses homologous recombination (Denchi and de Lange, 2007; Hockemeyer et al., 2006; Palm et al., 2009; Wu et al., 2006). Furthermore, the telomeric overhang invades the duplex region, forming a t-loop (Griffith et al., 1999) and thereby blocking ATR and ataxia telangiectasia mutated (ATM) signaling, which is essential to prevent the chromosome end from being incorrectly recognized as a DNA double-stranded break (de Lange, 2009).

Because of the end-replication problem, the ends of chromosome shorten with each round of DNA replication in all somatic cells (Harley et al., 1990; Watson, 1972). The progressive telomere attrition results in replicative senescence, growth arrest, or apoptosis (Karlseder et al., 1999; Smogorzewska and de Lange, 2002). Cancer cells, however, overcome this barrier mostly (85%–90%) by upregulating telomerase activity to sustain the telomere length (Kim et al., 1994; Shay and Bacchetti, 1997). Nevertheless, a significant subset (10%–15%) of cancers that are telomerase negative lengthen telomeres by a telomerase-independent mechanism, termed alternative lengthening of telomeres (ALT) (Bryan et al., 1995, 1997; Cesare and Reddel, 2010). ALT is likely mediated by homologous recombination (HR) mechanisms (Dunham et al., 2000; Lundblad and Blackburn, 1993; Varley et al., 2002). Numerous proteins involved in telomere function, HR, DNA damage repair, and DNA replication are associated with ALT (Cesare and Reddel, 2008). Therefore, all cancer cells exhibit indefinite lifespan supported by either the telomerase-catalyzed extension or ALT-mediated lengthening of telomeres. Because of this common feature of all cancers, telomeres and telomere-associated proteins have been attractive drug targets for anticancer therapy (Shay and Bacchetti, 1997; Shay and Wright, 2002; Tárkányi and Aradi, 2008).

The telomeric overhang presents a highly vulnerable target that can be misrecognized to induce a DNA damage response that can lead to chromosome fusion and erosion (d'Adda di Fagagna et al., 2004; Harley et al., 1990; Lingner et al., 1995; Palm and de Lange, 2008; Shampay et al., 1984). Therefore, the capping and protection of the telomeric overhang is of utmost importance for genome integrity. From *Schizosaccharomyces pombe* to humans, the overhang is specifically bound by the shelterin component POT1, which prevents single-stranded DNA (ssDNA)-stimulated repair and recombination (Denchi and

 

de Lange, 2007; Hockemeyer et al., 2005). Furthermore, POT1 regulates access to the overhang to facilitate complete chromosome replication (Colgin et al., 2003; Lei et al., 2005; Shakirov et al., 2005; Ye et al., 2004).

Although many proteins need to gain access to the telomere overhang for maintenance and lengthening, the G-quadruplex structure that can form in successive repeats of TTAGGG may serve as a structural barrier to protein access. Recent reports provide strong evidence that G-quadruplexes form in cells, including at telomeres (Biffi et al., 2013; Paeschke et al., 2011, 2013; Sfeir et al., 2009; Vannier et al., 2012). Structural studies show that in the presence of $K^+$ or $Na^+$ ions, four TTAGGG repeats fold into stable G-quadruplexes consisting of three tetrads of four guanines interacting via Hoogsteen base pairing (Hardin et al., 1991, 1992). Oligonucleotides with four TTAGGG repeats are poor substrates for telomerase because of G-quadruplex folding (Wang et al., 2011). However, the current view of telomeric overhang structure is incomplete because it derives largely from images of static molecules with four or fewer telomeric repeats.

Using highly sensitive single-molecule techniques, we have examined the folding behavior of overhangs with varying numbers of telomeric repeats (four to eight) and how this behavior relates to overhang accessibility to proteins involved in telomere processing. We observed that the overhang structural dynamics increased as a function of length and that the dynamic properties influenced overhang accessibility. We investigated loading of several ALT-associated proteins, along with POT1 and telomerase, both of which bind telomere overhangs in a sequence-specific manner. Our results reveal that overhangs with four TTAGGG repeats fold into a stable G-quadruplex and are poor substrates for protein loading. In contrast, five to seven repeat overhangs exhibit significantly higher dynamics and corresponding accessibility to most of the molecules tested. Collectively, our observations point to the importance of the dynamics of G-quadruplex structures located at 3′ overhangs in governing the processing of telomeres by proteins involved in telomere-lengthening mechanisms.

## RESULTS

### Telomere Overhangs Longer than Four Repeats Display Multiple Conformations and Dynamics

Although numerous studies have examined the folding kinetics of human G-quadruplex (GQ), studies of physiologically relevant telomeric substrates that have more than four repeats of TTAGGG are limited (Bauer et al., 2011; Lane et al., 2008; Vorlíčková et al., 2005). Melting temperature and circular dichroism experiments have suggested that GQs are blocks that resemble beads on a string and that they can move independently of each other and are constrained only by connecting linkers (Petraccone et al., 2011; Yu et al., 2006). In addition, molecules with telomeric repeats in multiples of four exhibit increased enthalpy and entropy arising from stable GQ formation (Yu et al., 2006). On the contrary, a previous atomic force microscopy (AFM) study showed that long telomeric 3′ overhangs did not form the maximum number of GQs. Rather, they were dispersed, suggesting that GQ folding of overhangs longer than four repeats may be dynamic (Wang et al., 2010).

To investigate the effect of telomere repeat length on GQ conformation, we prepared a series of 3′ overhang DNA substrates with varying numbers of TTAGGG repeats from four to eight, which we refer to as G4–G8 hereafter. Each DNA was labeled with two fluorescent dyes, Cy3 and Cy5, at both ends of the ssDNA for measuring fluorescence resonance energy transfer (FRET). FRET, as a molecular ruler, reports on the folding status of the telomeric overhang such that a high FRET signal indicates GQ folding in G4 DNA (Figure 1A). In 100 mM KCl, we obtained one, two, and four FRET peaks for molecules with four (G4), five (G5), and six (G6) telomeric repeats, respectively (Figure 1B). Each FRET histogram was built from FRET values of over 5,000 individual molecules. We interpret the discrete FRET peaks as reflecting formation of one, two, and four conformations in G4, G5, and G6, respectively. It is plausible that G5, for example, folds up in two different ways, i.e., GQ consisting of repeats 1–4 or 2–5, yielding two distinct FRET states. With seven telomeric repeats (G7), we observed a broad FRET histogram, likely because of formation of multiple conformations arising from various ways of GQ folding that yield a wide range of dye to dye distance. For G8, we also obtained a broad FRET distribution, yet with a prominent high FRET peak. Based on the total length of single-stranded DNA of 48 nucleotides in G8, this high FRET far exceeds the expected FRET value (below 0.2) in this buffer condition (Murphy et al., 2004). Therefore, the unusually high FRET in G8 is likely due to the formation of two GQs from two sets of four repeats (Figure 1B).

To confirm that the high FRET state represents folded GQ DNA, we examined overhang dynamics in various monovalent salts. $K^+$ and $Na^+$ stabilize GQ folds by coordinating in the central channel of the tetrads; however, the smaller $Li^+$ ions do not support GQ folding (He et al., 2005; Wong and Wu, 2003). As expected, 100 mM NaCl induced similar distributions of GQ conformations for G4–G8, as we obtained for 100 mM KCl conditions (Figure S1 available online). We note that the slight differences obtained for NaCl and KCl are likely due to different conformations of GQ in sodium and potassium ion as reported previously (Ambrus et al., 2006). In contrast to KCl and NaCl, 100 mM LiCl induced broad FRET peaks for all overhang lengths with overall lower FRET values, reflecting no discrete folding of GQs. To test the sequence-dependent folding of GQ, we prepared the G4 and G8 mutants, which bear TTAGCG (instead of TTAGGG) at the fourth and eighth repeats, respectively. Both mutants, which differ from G4 and G8 by only a single nucleotide, resulted in a completely different FRET distribution that reflects lower a FRET unfolded state, similar to the LiCl condition. This confirms that the high FRET peak for the G8 overhang in KCl and NaCl likely represents two folded GQs, because mutating the last repeat eliminates the high FRET peak, even though a GQ could still form between repeats 1 and 7.

Next, we sought to probe the real-time dynamics in G4–G8 DNA by analyzing the single-molecule traces. The representative single-molecule trace for G4 shows that it stays in one high FRET state, which is consistent with the histogram. The G5 and G6 overhangs, however, display two and four FRET states in exchange, respectively, likely representing different conformations arising from alternative folding of GQ. G7 and G8 traces exhibit many more FRET states, reflecting dynamic exchanges among multiple conformations (Figure 1C). In addition, the rate at which

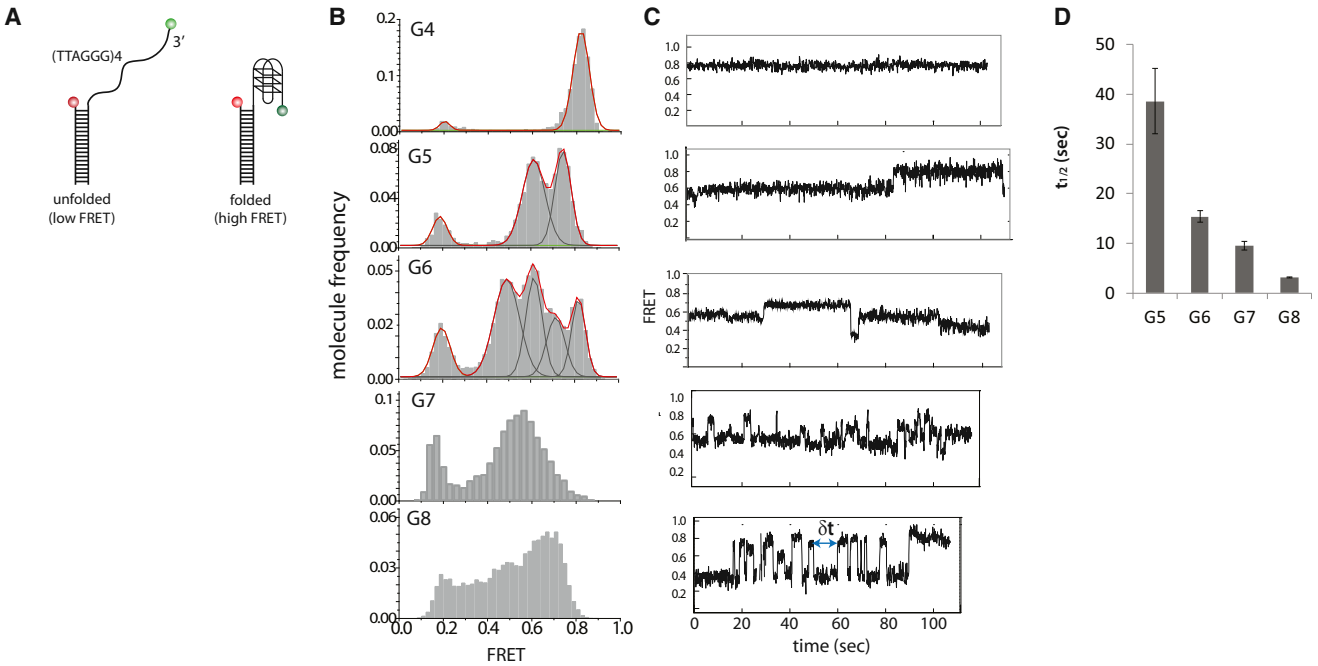


**Figure 1. Telomere Overhangs Longer than Four Repeats Display Multiple Conformations and Dynamics**

(A) Schematic of DNA used for single-molecule FRET. Two dyes, Cy3 and Cy5, are attached to both sides of four repeats of TTAGGG. High FRET and low FRET correspond to folding and unfolding of GQ, respectively.

(B) Single-molecule frequency histograms of DNA with four, five, six, seven, and eight repeats of TTAGGG. The red outlines are the summations of one, two, and four Gaussian fits for G4, G5, and G6, respectively.

(C) Representative single-molecule trace for G4–G8.

(D) Plot of half time ($t_{1/2}$) obtained from fitting dwell times to exponential decay. (Dwell times are denoted by a blue arrow in single-molecule trace.)

conformations exchange becomes faster for longer overhangs. To quantify this effect, we collected dwell times ($\delta t$, Figure 1C) from about 200 molecules for each DNA and fitted the data to an exponential decay. The half-life ($t_{1/2}$) obtained from the fit reveals that the fastest dynamic in G8 is one order of magnitude higher than the slowest time obtained for G5. These faster dynamics observed for the longer overhangs indicate that increased repeat number induces more rapid exchanges (Figure 1D; Figure S1). Taken together, telomeric overhangs longer than four repeats exhibit dynamic folding states, and the longer lengths induce more complex conformations and faster dynamics. Interestingly, despite the fast conformational dynamics, overhangs with eight repeats display frequent transitions to the high FRET state, likely arising from the formation of two GQs.

## GQ Dynamics Modulate Overhang Accessibility to Complementary DNA

A short antisense strand of the telomeric sequence is frequently used to test unfolding of GQ structures by forming duplex DNA with the unfolded molecules (Wang et al., 2010; Zaug et al., 2005). In addition, antisense telomeric DNA exists in ALT cells in the form of c-circles and has been employed as a specific and quantifiable marker of ALT activity in vivo (Henson et al., 2009). We applied a similar 12-nucleotide (nt) C2 complementary antisense $(CCCTAA)_2$ molecule in excess (10 nM) to test the accessibility of the G4–G8 overhangs. We note that the annealing experiment was performed at room temperature without adding any external source of heat. The FRET values from more than 1,000 molecules were taken before and 10 min after the addition of C2 DNA. Binding of C2 is expected to result in a FRET decrease (Figure 2A). The FRET histograms were prepared from data collected before and after C2 incubation, shown in dark gray and light blue, respectively (Figure 2B). As a positive control, we included G3TTAG, a G4 overhang devoid of the two terminal Gs that cannot fold into GQ (Hwang et al., 2012). The histogram for G3TTAG, G6, and G7 showed a substantial shift to lower FRET values, whereas G4, G5, and G8 remained nearly unchanged after C2 incubation (Figure 2B). The lower FRET states upon C2 binding for the G6 and G7 overhangs are also broadly distributed, reflecting multiple conformations as seen before. The percentage of accessibility was calculated by subtracting the histogram before C2 addition from the histogram after the addition of C2, indicating the percentage of molecules that have C2 bound (Figures S2A and S2B). The same experiment was performed at an ensemble level using a fluorometer, from which the accessibility was calculated by the percentage of change in FRET value before and after C2 addition. The same pattern of accessibility emerged from the two sets of data, both pointing to a limited accessibility in G4, G5, and G8 molecules and increased accessibility for G6 and G7. G5 was slightly more accessible than G4, which is consistent with increased folding dynamics compared with G4. As evident from the data, G3TTAG represents the most accessible substrate because of the lack of GQ folding. Despite high dynamics

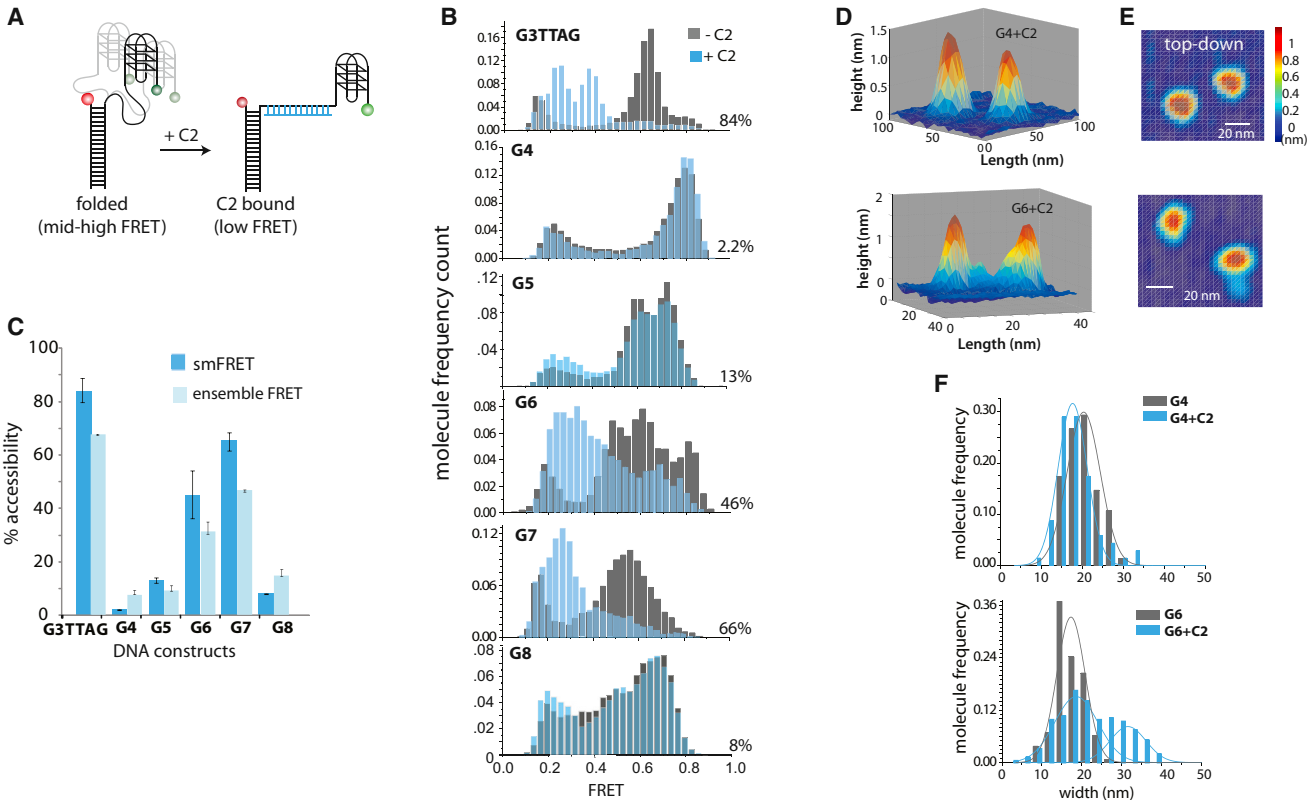


**Figure 2. GQ Dynamics Modulate Overhang Accessibility to Complementary DNA**

(A) Schematic of complementary 12-mer, C2, binding to single-stranded portions of the telomeric overhang repeats.

(B) Frequency count histograms before and after binding of C2 to G3TTAG and G4–G8.

(C) Percentage of accessibility calculated for single-molecule and ensemble FRET.

(D and E) Example contour plots of two G4 molecules and two G6 molecules incubated with C2, imaged with AFM. (D) Side view. (E) Top-down view.

(F) Width distribution histograms of molecules for G4 and G6 before and after the addition of C2 collected by AFM imaging.

in folding, G8 was largely inaccessible, likely because of the ability to form two GQs.

To determine whether stable GQ folding was responsible for the limited C2 binding to G4, G5, and G8, we repeated the experiments in the presence of 100 mM NaCl and 100 mM LiCl. As expected, the similar pattern of accessibility was also obtained in the 100 mM NaCl condition where GQ structures resemble that of KCl condition (Figure S2B). In LiCl, where the GQ folding is unstable, the C2 accessibility to G4, G5, and G8 was as high as for the control G3TTAG substrate (Figure S2C). Furthermore, the G4 and G8 mutants with a single-nucleotide change to prevent one or two stable GQ folds, respectively, also displayed high accessibility to C2 (Figure S2D). In both the LiCl and mutant cases, the lack of stable GQ folding is likely responsible for the increased accessibility to C2 strand binding for all substrates.

To gain structural insight into C2 binding, we examined GQ images captured by AFM. We compared the least accessible substrate, G4, with one of the most accessible substrates, G6. The G4 and G6 molecules preincubated with C2 appear as a sharp peak representing the folded GQ (Figure 2D). We note that the two peaks in Figure 2D represent two individual G4 molecules, both of which yield a single sharp peak, and the same is true for G6 peaks. Unlike a single peak arising from G4, the G6 peak possesses a shoulder peak that likely represents C2 binding (Figure 2E). We confirmed that the shoulder peak only occurs in G6 incubated with C2, but not in G4. This is shown in the histograms where the widths of G4, G4+C2, G6, and G6+C2 are collected from approximately 100 molecules and plotted as a molecular frequency (Figure 2F). These data provide structural evidence that although G6 is accessible to C2 binding, the G4 molecule is not.

## GQ Conformation Influences RAD51 Access

RAD51 is a key player in the homology-directed repair that triggers ALT pathway (Oganesian and Karlseder, 2011). Furthermore, the inhibition of RAD51 synthesis leads to telomere erosion and chromosome fusion, suggesting an important role of RAD51 in telomere maintenance (Tarsounas et al., 2004). We sought to examine whether GQ folding and dynamics modulate RAD51's ability to bind and resolve the GQ conformation (Figure 3A, top). RAD51 addition to all substrates induced a substantial shift in FRET, except for the G4 substrate. The emergence of low FRET states upon RAD51 addition in all cases is likely due to the filament formation expected from RAD51 binding (Figure 3B). G4 showed the lowest accessibility, suggesting the presence of a stable GQ fold that limits RAD51 binding.

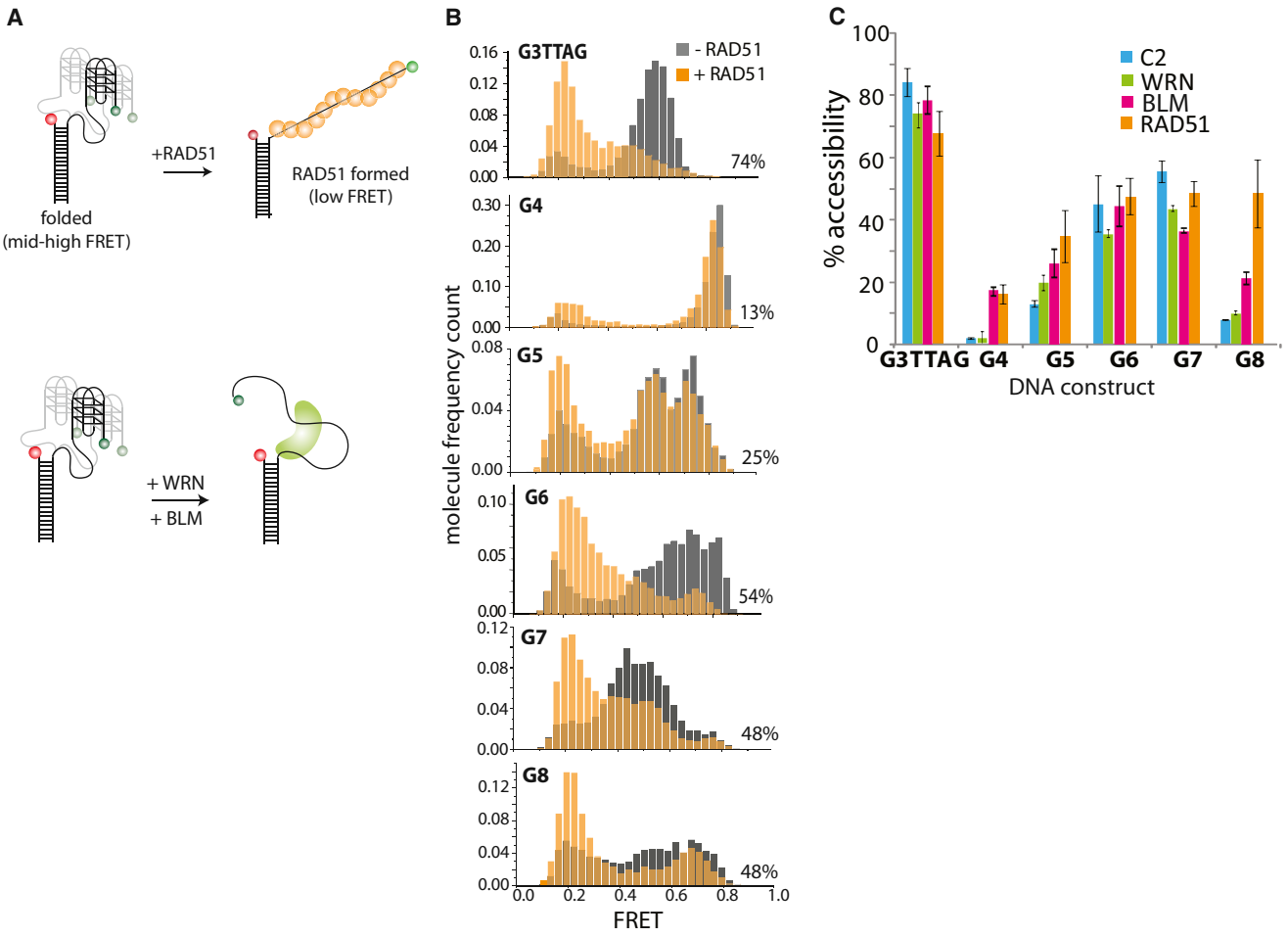


**Figure 3. GQ Conformation Controls RAD51, WRN, and BLM Access**

(A) Schematic of RAD51 and RecQ helicases (WRN and BLM) to DNA.

(B) Frequency count histogram before and after addition of RAD51 on G3TTAG and G4–G8.

(C) Summary plot comparing percentage of accessibility between RAD51, WRN, BLM, and C2 for increasing repeat numbers of the telomere overhang.

The percentage of accessibility resulting from all overhang lengths shows an overall resemblance to C2 antisense accessibility with the largest difference observed in G8 (Figure 3C, orange bars). Unlike the case of C2 binding, G8 yields high accessibility to RAD51, likely because of the small DNA binding size of RAD51. RAD51 is a structural homolog of the *Escherichia coli* RecA recombinase that engages 3 nt (Chen et al., 2008; Shin et al., 2003) of DNA per protein monomer to form a filament (Arata et al., 2009; Hilario et al., 2009; van Mameren et al., 2009). Therefore, the higher accessibility shown for RAD51 than C2 may be explained at least in part by the different lengths of single-stranded DNA required for RAD51 (3 nt) compared with C2 (12 nt) binding.

## WRN and BLM Access to Telomeric Overhangs Depends on the GQ Folding Dynamics

Human RecQ family helicases Werner (WRN) and Bloom (BLM) can unwind GQs in vitro, with high specificity (Liu et al., 2010; Mohaghegh et al., 2001). BLM, in conjunction with RAD51, can interact with TRF2 in ALT-activated cells to promote telomere elongation (Stavropoulos et al., 2002), whereas WRN is directly involved with telomeric recombination in the ALT pathway (Mendez-Bermudez et al., 2012). However, both WRN and BLM require a 3′ ssDNA tail to unwind a G-quadruplex (Mohaghegh et al., 2001). To determine whether overhang length influences WRN and BLM loading and activity, we applied both proteins to the overhang substrates (G4–G8) and monitored potential FRET decreases as indicative of protein loading and GQ unwinding (Figure 3A, bottom). The FRET histograms collected after addition of WRN and ATP displayed a negligible (<10%) shift for G4 and G8, whereas a significant change was observed for G5, G6, and G7 (Figure S3A). The same pattern was also seen for BLM (Figure S3B). To further examine the ATP dependence of the protein loading, we applied WRN to the same set of DNA constructs in the absence of ATP and in the presence of the nonhyrolysable analog ATPγS. The accessibility data indicate that WRN does not bind in the absence of ATP, but the binding occurs to a similar degree in the ATP condition compared with the presence of ATPγS, albeit reduced (Figure S3C). Taken together, we demonstrate that the GQ folding in G4 and G8 is the

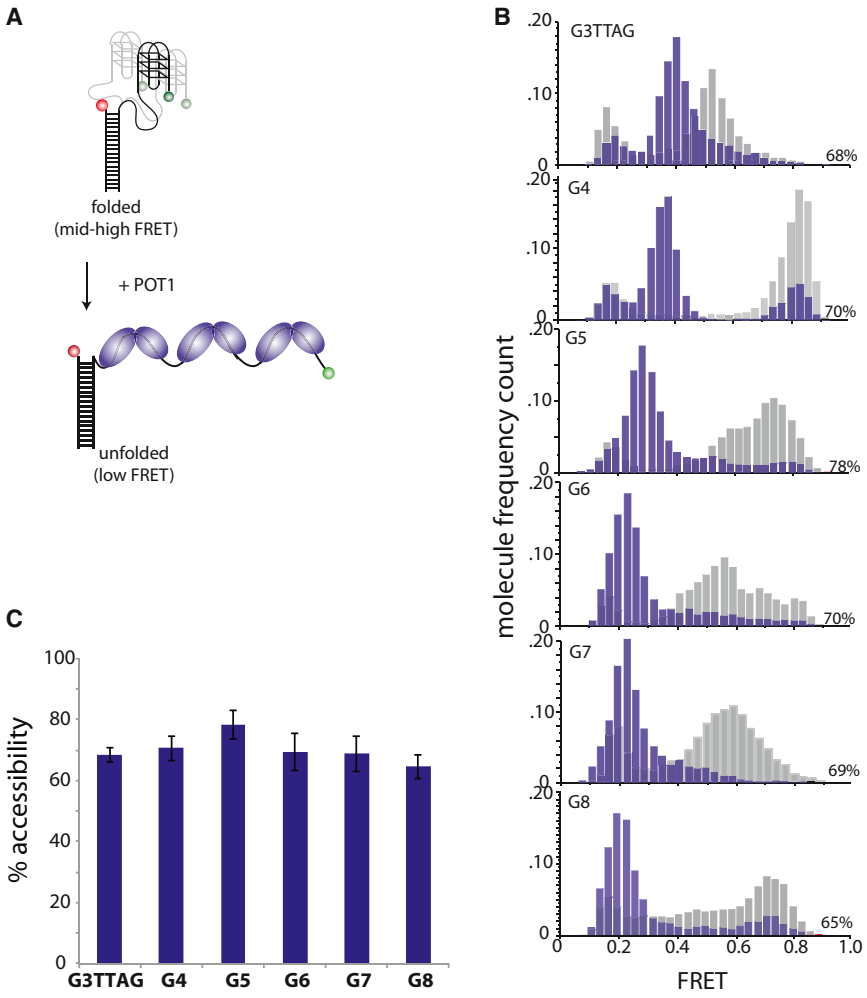


**Figure 4. POT1 Binding Is Independent of GQ Folding and Overhang Length**

(A) Schematic of POT1 unfolding the telomeric DNA.

(B) Molecule frequency count histograms before and after addition of POT1 for G3TTAG and G4–G8 DNA.

(C) Plot of percentage of accessibility for POT1 binding to increasing number of telomere overhang.

least accessible to RecQ helicase loading, whereas G5–G7 yield substantially higher accessibility, similar to C2 antisense binding (Figure 3C).

## POT1 Binding Is Independent of GQ Folding and Overhang Length

POT1 (Protection of Telomeres 1) is a member of shelterin complex that guards and controls the single-stranded telomeric overhang (Denchi and de Lange, 2007). POT1 engages with the telomeric overhang in a sequence-specific manner (TTAGGGTTAG) as clearly demonstrated by the high resolution structure and biochemical characterization (Lei et al., 2004). Recently, we reported that POT1 binds and thereby unfolds GQ in a stepwise fashion in which one monomer binds TTAGGGTTAG in two successive steps (Hwang et al., 2012). In the previous study, we used shorter overhang lengths, G2–G4, to focus on the detailed monomer binding steps. In the current study, we use G4–G8 to test whether POT1 binding is influenced by GQ folding and dynamics exhibited in the longer overhang (Figure 4A). The FRET histogram obtained after adding POT1 clearly shows that POT1 binding occurred to a similar degree for all overhang lengths (Figures 4B and 4C). POT1 displayed a binding mode that was independent of the inherent conformational states and dynamics governed by the repeat number, in contrast to the repeat number-dependent loading exhibited by C2, RAD51, WRN, and BLM.

## Telomerase Loading and Extension Activity Is Modulated by GQ Dynamics

GQ structures inhibit telomerase activity (Salazar et al., 1996; Zahler et al., 1991), hence the anticancer therapy efforts in developing drugs that stabilize GQ. The sequence-specific binding of telomerase to the telomere is achieved by the complementarity between the telomeric overhang and the RNA template embedded in the catalytic site of telomerase (Weinrich et al., 1997). In this respect, telomerase shares similarity with POT1. To examine telomerase activity, we used an established telomerase isolation protocol. HEK293T cells were transfected with Flag-tagged telomerase overexpression plasmids (generous gift from Tom Cech) (Latrick and Cech, 2010). The cell lysate was applied to a single-molecule surface pretreated with anti-Flag antibody (α-Flag) to pull down the Flag-tagged telomerase (Jain et al., 2011). The pull-down efficiency was tested by applying the primary antibody against telomerase followed by red (Alexa 647)-labeled secondary antibody (Figure 5A). The red fluorescent spots appeared only when all the components were present and were not detected above background when any of α-Flag, cell lysate, or primary antibody was omitted, indicating the highly specific capture of telomerase (Figures 5B and 5C).

We used this platform to evaluate overhang accessibility by applying green (Cy3)-labeled DNA followed by the primary and red-labeled secondary antibody used above (Figure 5D). By colocalizing the green and red signals, we were able to count the number of telomerase molecules occupied by the corresponding DNA. The fraction of red molecules that colocalize with green was used to calculate the percentage of occupancy of telomerase bound to DNA (Figure 5E). The resulting bar graph reveals that G4 and G8 are less occupied by telomerase than G3TTAG, G6, and G7, indicating a similar pattern of accessibility seen for C2 and the helicases. The limited occupancy by G4 and G8 coupled with the enhanced binding by G6 and G7 points to a

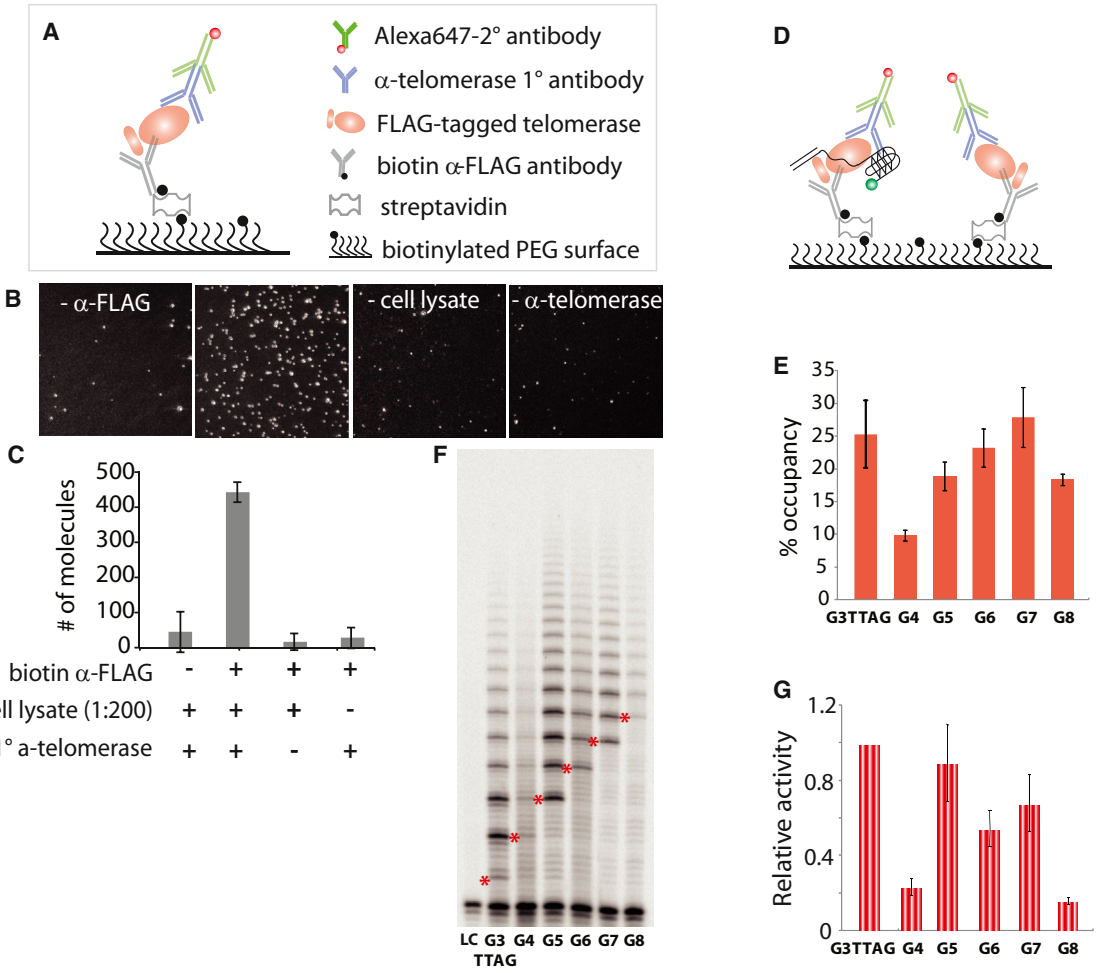


**Figure 5. Telomerase Loading and Extension Activity Is Modulated by GQ Dynamics**

(A) Schematic of single-molecule pull-down of overexpressed telomerase (Flag-tagged) from HEK293T cells.

(B and C) Images (B) and quantification (C) of molecules pulled down demonstrating the specificity of telomerase capture.

(D) Schematic of colocalization of telomerase (Alex 647-labeled antibody) and Cy3-labeled telomeric DNA.

(E) Percentage of occupancy of DNA to telomerase calculated by the percentage of colocalization.

(F) Gel image from primer extension assay with various repeat length constructs.

(G) Quantification of extension activity by using ImageJ and ImageQuant.

loading mechanism of telomerase that relies on the conformational dynamics of the telomeric overhang.

Next, we asked whether the telomerase extension activity reflected the overhang length dependency of telomerase binding. We performed a modified version of primer extension assay in which Flag-telomerase was immunoprecipitated onto α-Flag-coated beads, and the telomere extension was stimulated by adding the individual DNA template and mix of dNTPs including radiolabeled dGTP. The reaction was carried out in the same buffer condition used for the single-molecule assay at 37°C for 1 hr until the reaction was quenched and analyzed by 12% PAGE (Figure 5F). We quantified the product of telomerase extension by ImageJ and ImageQuant software. The total intensity collected for each DNA was normalized by the total intensity obtained for G3TTAG, a positive control DNA template that leads to the highest extension activity (Berman et al., 2011; Latrick and Cech, 2010). As shown, the telomerase extension also exhibits the similar length dependency with limited activity for G4 and G8 and a significantly higher activity measured for G5–G7 (Figure 5G), suggesting that the telomerase loading to telomeric overhang may contribute to the level of telomerase extension. The slight differences observed between the accessibility of DNA and the telomerase activity can be due to several factors. It is possible that not all the substrates bound to telomerase in the single-molecule surface are productive, i.e., engaged in correct orientation or position sufficient to yield telomerase activity. Further, the ability of G8 to fold into two GQ structures may impact the ability of telomerase to engage the overhang in the enzyme active site for telomere extension.

## DISCUSSION

Early work suggests that the formation of GQ at the telomeric overhang limits access of telomerase and other telomere binding

proteins (Burger et al., 2005; Gomez et al., 2006a, 2006b; Phatak et al., 2007; Tahara et al., 2006). Furthermore, dimethylsulfate footprinting study demonstrated that the GQ preferentially forms at the end of a 3′ overhang rather than at the internal positions, suggesting that the GQ formation at the end position may inhibit telomerase and ALT-mediated telomere lengthening (Tang et al., 2008). Using single-molecule approaches, we discovered that the telomere overhang length greatly influences the dynamics of GQ unfolding. We sought to examine how DNA conformational dynamics influences the accessibility of telomeric overhangs to proteins that are relevant for telomere protection and lengthening. We observed that in general, increasing overhang length led to increased conformational dynamics and greater accessibility to protein loading. However, we also note interesting exceptions. First, the overhangs consisting of multiples of four repeats were the least accessible regardless of length. We further confirmed this effect by control measurements. In ionic conditions that stabilize GQ (NaCl and KCl), the G4 and G8 remain inaccessible, whereas they become fully accessible to complementary DNA (C2) binding in LiCl buffer, which destabilizes GQ. Further, the GQ folding is disrupted by a single-nucleotide mutation in both G4 and G8 cases, making them fully accessible to C2 binding. Second, the binding of the telomeric protein POT1 was not influenced by overhang length or dynamics. In light of the intimate contact between POT1 and telomeric overhang DNA displayed in their structure (Lei et al., 2004), it is not surprising to observe that POT1 can actively disrupt the GQ folding. Collectively, these studies indicate that telomere overhang length modulates telomere processing with the exception of POT1.

The single-molecule FRET employed here is an ideal approach in several respects. First, the range of distance change induced by GQ folding and unfolding is within the FRET sensitive detection range. Second, single-molecule detection enables the resolution of various conformers of GQ exhibited by the different overhang lengths. Although we cannot identify the exact conformations represented by different FRET values, the overall histogram obtained for G4, G5, G6, G7, and G8 reveals one, two, four, and multiple states, respectively, as can be expected from alternate pairings of G-triplets (Figure 1B). Although different FRET values observed in G5–G7 do not inform us about the exact conformations, we predict that the GQ formed by neighboring G-triplets contributes to the various folding states. For example, there are three ways that G6 can fold by pairing up of repeats 1–4, 2–5, and 3–6, and the fourth state can result from a flanking of the single-stranded portion of DNA. Third, single-molecule traces reveal the real-time molecular dynamics of GQ as it undergoes conformational changes by itself (Figure 1C). Individual single-molecule traces of G5–G8 reveal that they are in dynamic exchange with alternate conformers and that the rate of exchange is accelerated as the repeat number increases (Figures 1C and 1D). Although the conformers appear to be evenly distributed among different conformers in G5–G7, G8 displays a pronounced high FRET peak that exceeds the other states (Figure 1B). We interpret this high FRET as arising from two GQs forming on G8, which in turn yields low accessibility to several proteins tested herein. Consistent with this, mutation of the eighth repeat prevents two GQs from folding and eliminates this high FRET peak, even though a single GQ fold can still form among repeats 1–7. It is interesting to note that G8 exhibits both the high propensity for folding and the fast dynamic behavior. Although small proteins such as RAD51 gains access to such construct, most other proteins had significantly reduced access to G8.

The conformational dynamics of DNA and its length-dependent accessibility to various proteins may have implications for when the telomeric overhang becomes exposed during replication, for example. Although it may be transient, the free single-stranded overhang is expected to exhibit conformational dynamics; however, proteins such as POT1, telomerase, and ALT-associated proteins will compete for binding to the same overhang. Based on our result, the number of TTAGGG repeats at the very end of an individual telomere will influence its conformational dynamics and the corresponding level of accessibility to the available proteins. Depending on which protein gains access, the telomere will face different outcomes. If the end is bound by telomerase, it will be extended, whereas if the end is accessed by RAD51, the end may undergo a homology directed repair pathway (Cesare and Reddel, 2008; Henson et al., 2002). However, in normal somatic cells, it is likely that the telomeric end is readily occupied by POT1. In a cell, the folding of a telomeric overhang into a GQ converts it to substrate for binding by various proteins that can interact with GQ structures and compete for loading. However, evidence shows that POT1 can effectively compete for loading on the telomeric overhang because of telomere tethering by shelterin TPP1-TIN2 (Takai et al., 2011). TPP1 also recruits telomerase to the telomeres in a cell cycle-regulated matter (Zhang et al., 2013). Therefore, the status of the shelterin complex at the telomere contributes to protein recruitment and loading on the overhang. Our data indicate that overhang structural dynamics also contribute to regulating protein accessibility. Importantly, we showed that POT1 can load on telomeric overhangs that are prefolded in a GQ, including the G4 and G8 substrates (Figure 4).

Taken together, we have provided in vitro evidence that GQ folding at the 3′ end of the telomeric overhang plays a critical role in controlling protein access. All ALT-associated proteins tested here show the length-dependent loading that resembles C2 binding with the exception of RAD51, which readily gains access to G8, which renders low accessibility to all other proteins tested. In contrast, POT1 bound the G4–G8 substrates with equal efficiency, clearly indicating a different binding mode that leads to active disruption of GQ (Hwang et al., 2012; Wang et al., 2010; Zaug et al., 2005). A better understanding of the mechanisms for regulating chromosome end structure and accessibility will help identify new targets for anticancer therapies, with improved specificity for telomeres. Furthermore, our single-molecule platform provides a screening tool for testing the current and future generation GQ ligands, thereby assessing anticancer drugs with single molecular sensitivity. Many factors likely contribute to the regulation of telomere lengthening by ALT or telomerase, and our data provide evidence that telomere overhang length is one factor that may contribute to this regulation.

## EXPERIMENTAL PROCEDURES

### Ensemble C2 Measurements

Bulk measurements were performed at room temperature (24 ± 1°C) in a standard, G-quadruplex formation reaction condition: 100 mM KCl, 100 mM Tris,

with a 10 nM partial duplexed telomeric DNA sample. The reaction was initiated with 1 nM of C2 DNA. FRET efficiency, E, was monitored with a fluorescence spectrophotometer (Cary Eclipse, Varian). Accessibility of G-quadruplex DNA was determined by comparing DNA-only FRET efficiency, $E_{DNA}$, with steady-state efficiency after C2 addition, $E_{C2+DNA}$ according to:

$$\frac{E_{DNA} - E_{C2+DNA}}{E_{DNA}}.$$

### AFM Sample Preparation and Imaging

DNA substrates were diluted to 2 ng/μl in reaction buffer with additional 10 mM $MgCl_2$. All samples were incubated at room temperature for 15 min. Samples were deposited on freshly cleaved mica (Ted Pella), followed by a wash with deionized water and drying with nitrogen. Imaging was performed on a Cypher AFM (Asylum Research) in tapping mode. AC160TS AC mode silicon probes with spring constants of ~42 newtons/m and resonance frequencies of 300 kHz were used. Images were captured at a scan size of 1 μm by 1 μm with a resolution of 1,024 by 1,024 pixels.

### Protein Purification and Reaction Conditions

RAD51 was purified in a way similar to that described previously (Sigurdsson et al., 2001). Single-molecule experiments were done at 37°C and used 1 μM RAD51 with reaction buffer containing 50 mM KCl, 1 mM $MgCl_2$, and 1 mM ATP. The purified hetrotrimer replication protein A (RPA) was a kindly provided by Dr. Walter Chazin (Vanderbilt University) (Arunkumar et al., 2005). The reaction used 1 μM RPA with 100 mM KCl and 10 mM Tris. WRN proteins were purified as described previously (Opresko et al., 2009). Reactions were performed in 25 mM KCl, 1 mM $MgCl_2$, 10 mM Tris, pH 7.5, and 2 mM ATP. BLM was purified as described previously (Bussen et al., 2007), and single-molecule reactions were performed with 100 nM BLM in the presence of 3 mM $MgCl_2$, 20 mM Tris, pH 7.6, 50 mM KCl, and 2 mM ATP.

### Gel Mobility Shift Assay

The 10 nM partial duplex telomeric overhang was mixed with and without 200 nM RPA with Cy5 dyes at the junction and incubated for 15 min at 37°C with 2 mM $MgCl_2$, 10 mM Tris, pH 7.6, and 50 mM KCl. The reaction mixture was loaded and run on a 6% acrylamide gel at 65 V for 2 hr with 0.5×TBE running buffer. Analysis in ImageJ was used to quantitate accessibility percentages by taking the area of DNA with RPA and normalizing it to the areas of the sum of DNA with RPA and DNA alone.

### Telomerase Overexpression

Overexpression of telomerase was carried out using modification to an established protocol (Cristofari and Lingner, 2006). Cell lysate containing recombinant telomerase was reconstituted in HEK293T cells by overexpressing hTR and 3×FLAG-tagged human telomerase reverse transcriptase (hTERT) genes in pBS-U1-hTR and pVan107, respectively (generous gifts from Dr. Thomas Cech). Cells were grown to 90% confluency containing Dulbecco's modified Eagle's medium (Gibco) supplemented with 10% FBS (Gibco) and 1% penicillin-streptomycin (Gibco) at 37°C and 5% $CO_2$. Cells were transfected with 10 μg of pBS-U1-hTR plasmid and 2.5 μg of pVan107 plasmid diluted in 625 μl of Opti-MEM (Gibco) using 25 μl of Lipofectamine 2000 (Invitrogen) diluted in 625 μl of Opti-MEM according to the manufacturer's instructions. Cells were allowed to grow for 48 hr post-transfection, at which point they were trypsinized and washed with phosphate-buffered saline and lysed using 500 μl of 3-[(3-cholamidopropyl)dimethylammonio]-1-propanesulfonic acid (CHAPS) lysis buffer (10 mM Tris-HCl, 1 mM $MgCl_2$, 1 mM EDTA, 0.5% CHAPS, 10% glycerol, 5 mM β-mercaptoethanol, 120 U of Promega RNasin plus, 1 μg/ml pepstatin, aprotinin, leupeptin, chymostatin, and 1 mM AEBSF). Cell lysate was then either flash frozen in liquid nitrogen and stored at −80°C or immunopurified.

### Immunopurification of Telomerase

Telomerase enzyme was immunopurified from cell lysate using anti-Flag M2 affinity gel (Sigma). Prior to addition of the affinity gel to the cell lysate, 40 μl of affinity gel beads were washed three times with 40 μl of 1× human telomerase buffer (50 mM Tris-HCl, pH 8, 50 mM KCl, 1 mM $MgCl_2$, 1 mM spermidine, 5 mM β-mercaptoethanol, and 30% glycerol) by centrifugation at 4,000 rpm for 1 min at room temperature followed by removal of the 40 μl of supernatant. Following washes, 80 μl of affinity gel-human telomerase buffer slurry was added to the 500 μl of cell lysate and placed on a rotator for 3 hr at 4°C. After centrifugation at 4,000 rpm and removal of liquid, the beads were washed three times with 1× human telomerase buffer, flash frozen in liquid nitrogen as 80 μl of bead slurry in 1× human telomerase buffer, and stored at −80°C.

### Single-Molecule Pull-Down of Telomerase and Colocalization with Telomeric DNA

We utilized single-molecule pull-down methods to pull down the telomerase complex from overexpressed telomerase cell lysate (Jain et al., 2011). Telomerase was isolated on the biotinated polyethylene glycol-coated quartz surface in the following order: streptavidin, 1:50 anti-Flag antibody (Sigma; mouse M2, F9291), 1:200 cell lysate, 1:100 primary hTERT antibody (Abcam; rabbit monoclonal), and 1:10,000 secondary antibody labeled with Alexa 647 (Jackson Immunoresearch; donkey anti-rabbit).

Each step was incubated for 15–30 min, and 200 μl of telomerase reaction buffer (50 mM Tris-Cl, pH 8, 50 mM KCl, 1 mM $MgCl_2$) was flowed in to wash out unbound molecules in between each addition. The channels without anti-Flag antibodies, primary antibodies, or cell lysate showed <50 fluorescent spots per imaging area of 2,500 $\mu m^2$, possibly because of surface impurities.

To check the binding affinity of telomerase to DNA, 1 nM of the partial duplex telomeric DNA labeled with Cy3 was incubated with the isolated telomerase on the surface prior to the addition of antibodies. It was then washed before the hTERT primary and Alexa 647 secondary antibodies were added.

### Telomerase Extension Assay

The telomerase extension assay was a modification of a previously described protocol (Zaug et al., 2010).The telomerase extension reaction mixture (20 μl) contained 1× human telomerase buffer (described above), 2 μl of 3,000 Ci/mmol $^{32}$P-dGTP (PerkinElmer), 0.058 mM dGTP, 10 mM dTTP, 10 mM dATP, 1 μM telomeric partial duplex DNA substrate, and 6 μl of immunopurified telomerase complex. Reactions were incubated for 1 hr at 30°C, then stopped with the addition of 2 μl 0.5 M EDTA, and heat inactivated at 65°C for 20 min. Prior to purification of the sample using an Illustra microspin G-25 column (GE Healthcare), 8.0 fmol of a 37-mer loading control was added followed by the addition of 15 μl of loading buffer (94% formamide, 0.1 × Tris-borate-EDTA [TBE], 0.1% bromophenol blue, 0.1% xylene cyanol) to 15 μl of sample. The heat-denatured (10 min, 100°C) samples were loaded onto a 10% denaturing acrylamide gel (8 M urea, 1 × TBE) for electrophoresis. $^{32}$P incorporation was imaged using a phosphor screen and a PhosphorImager (GE Healthcare). Total activity was quantitated using ImageJ and ImageQuant and normalized to a loading control as established previously (Jain et al., 2011; Latrick and Cech, 2010). Briefly, each band is individually quantitated, summed, and normalized to the activity seen with the G3TTAG construct.

## SUPPLEMENTAL INFORMATION

Supplemental Information includes three figures and can be found with this article online at http://dx.doi.org/10.1016/j.str.2014.03.013.

## ACKNOWLEDGMENTS

We thank Walter Chazin (Vanderbilt University) for generously providing recombinant human replication protein A (R01 GM65484), Thomas Cech (University of Colorado at Boulder) for the Flag-tagged telomerase overexpression plasmid, Noah Buncher for technical support on protein purification, Ankur Jain for his help with the telomerase pull-down assay, and Ramreddy Tippana for helpful discussions. Support for this work was provided by an NIH Director's New Innovator Award (343 NIH 1 DP2 GM105453 A) and the American Cancer Society (Research Scholar grant RSG-12-066-01-DMC) to S.M., the Linda Su-Nan Chang Sah Doctoral Fellowship to H.H., NIH grant RO1 ES015632 to P.S., and NIH grant ES0515052 and the David Scaife Foundation to P.L.O.

Received: November 27, 2013
Revised: February 7, 2014
Accepted: March 4, 2014
Published: May 15, 2014

 

## REFERENCES

Ambrus, A., Chen, D., Dai, J., Bialis, T., Jones, R.A., and Yang, D. (2006). Human telomeric sequence forms a hybrid-type intramolecular G-quadruplex structure with mixed parallel/antiparallel strands in potassium solution. Nucleic Acids Res. *34*, 2723–2735.

Arata, H., Dupont, A., Miné-Hattab, J., Disseau, L., Renodon-Cornière, A., Takahashi, M., Viovy, J.L., and Cappello, G. (2009). Direct observation of twisting steps during Rad51 polymerization on DNA. Proc. Natl. Acad. Sci. USA *106*, 19239–19244.

Arunkumar, A.I., Klimovich, V., Jiang, X., Ott, R.D., Mizoue, L., Fanning, E., and Chazin, W.J. (2005). Insights into hRPA32 C-terminal domain-mediated assembly of the simian virus 40 replisome. Nat. Struct. Mol. Biol. *12*, 332–339.

Bauer, L., Tlučková, K., Tóhová, P., and Viglaský, V. (2011). G-quadruplex motifs arranged in tandem occurring in telomeric repeats and the insulin-linked polymorphic region. Biochemistry *50*, 7484–7492.

Berman, A.J., Akiyama, B.M., Stone, M.D., and Cech, T.R. (2011). The RNA accordion model for template positioning by telomerase RNA during telomeric DNA synthesis. Nat. Struct. Mol. Biol. *18*, 1371–1375.

Biffi, G., Tannahill, D., McCafferty, J., and Balasubramanian, S. (2013). Quantitative visualization of DNA G-quadruplex structures in human cells. Nat. Chem. *5*, 182–186.

Bryan, T.M., Englezou, A., Gupta, J., Bacchetti, S., and Reddel, R.R. (1995). Telomere elongation in immortal human cells without detectable telomerase activity. EMBO J. *14*, 4240–4248.

Bryan, T.M., Englezou, A., Dalla-Pozza, L., Dunham, M.A., and Reddel, R.R. (1997). Evidence for an alternative mechanism for maintaining telomere length in human tumors and tumor-derived cell lines. Nat. Med. *3*, 1271–1274.

Burger, A.M., Dai, F., Schultes, C.M., Reszka, A.P., Moore, M.J., Double, J.A., and Neidle, S. (2005). The G-quadruplex-interactive molecule BRACO-19 inhibits tumor growth, consistent with telomere targeting and interference with telomerase function. Cancer Res. *65*, 1489–1496.

Bussen, W., Raynard, S., Busygina, V., Singh, A.K., and Sung, P. (2007). Holliday junction processing activity of the BLM-Topo IIIalpha-BLAP75 complex. J. Biol. Chem. *282*, 31484–31492.

Cesare, A.J., and Reddel, R.R. (2008). Telomere uncapping and alternative lengthening of telomeres. Mech. Ageing Dev. *129*, 99–108.

Cesare, A.J., and Reddel, R.R. (2010). Alternative lengthening of telomeres: Models, mechanisms and implications. Nat. Rev. Genet. *11*, 319–330.

Chen, Z., Yang, H., and Pavletich, N.P. (2008). Mechanism of homologous recombination from the RecA-ssDNA/dsDNA structures. Nature *453*, 489–494.

Colgin, L.M., Baran, K., Baumann, P., Cech, T.R., and Reddel, R.R. (2003). Human POT1 facilitates telomere elongation by telomerase. Curr. Biol. *13*, 942–946.

Cristofari, G., and Lingner, J. (2006). Telomere length homeostasis requires that telomerase levels are limiting. EMBO J. *25*, 565–574.

d'Adda di Fagagna, F., Teo, S.H., and Jackson, S.P. (2004). Functional links between telomeres and proteins of the DNA-damage response. Genes Dev. *18*, 1781–1799.

de Lange, T. (2009). How telomeres solve the end-protection problem. Science *326*, 948–952.

Denchi, E.L., and de Lange, T. (2007). Protection of telomeres through independent control of ATM and ATR by TRF2 and POT1. Nature *448*, 1068–1071.

Dunham, M.A., Neumann, A.A., Fasching, C.L., and Reddel, R.R. (2000). Telomere maintenance by recombination in human cells. Nat. Genet. *26*, 447–450.

Gomez, D., O'Donohue, M.F., Wenner, T., Douarre, C., Macadré, J., Koebel, P., Giraud-Panis, M.J., Kaplan, H., Kolkes, A., Shin-ya, K., and Riou, J.F. (2006a). The G-quadruplex ligand telomestatin inhibits POT1 binding to telomeric sequences in vitro and induces GFP-POT1 dissociation from telomeres in human cells. Cancer Res. *66*, 6908–6912.

Gomez, D., Wenner, T., Brassart, B., Douarre, C., O'Donohue, M.F., El Khoury, V., Shin-Ya, K., Morjani, H., Trentesaux, C., and Riou, J.F. (2006b). Telomestatin-induced telomere uncapping is modulated by POT1 through G-overhang extension in HT1080 human tumor cells. J. Biol. Chem. *281*, 38721–38729.

Greider, C.W., and Blackburn, E.H. (1987). The telomere terminal transferase of Tetrahymena is a ribonucleoprotein enzyme with two kinds of primer specificity. Cell *51*, 887–898.

Griffith, J.D., Comeau, L., Rosenfield, S., Stansel, R.M., Bianchi, A., Moss, H., and de Lange, T. (1999). Mammalian telomeres end in a large duplex loop. Cell *97*, 503–514.

Hardin, C.C., Henderson, E., Watson, T., and Prosser, J.K. (1991). Monovalent cation induced structural transitions in telomeric DNAs: G-DNA folding intermediates. Biochemistry *30*, 4460–4472.

Hardin, C.C., Watson, T., Corregan, M., and Bailey, C. (1992). Cation-dependent transition between the quadruplex and Watson-Crick hairpin forms of d(CGCG3GCG). Biochemistry *31*, 833–841.

Harley, C.B., Futcher, A.B., and Greider, C.W. (1990). Telomeres shorten during ageing of human fibroblasts. Nature *345*, 458–460.

He, F., Tang, Y., Wang, S., Li, Y., and Zhu, D. (2005). Fluorescent amplifying recognition for DNA G-quadruplex folding with a cationic conjugated polymer: A platform for homogeneous potassium detection. J. Am. Chem. Soc. *127*, 12343–12346.

Henson, J.D., Neumann, A.A., Yeager, T.R., and Reddel, R.R. (2002). Alternative lengthening of telomeres in mammalian cells. Oncogene *21*, 598–610.

Henson, J.D., Cao, Y., Huschtscha, L.I., Chang, A.C., Au, A.Y., Pickett, H.A., and Reddel, R.R. (2009). DNA C-circles are specific and quantifiable markers of alternative-lengthening-of-telomeres activity. Nat. Biotechnol. *27*, 1181–1185.

Hilario, J., Amitani, I., Baskin, R.J., and Kowalczykowski, S.C. (2009). Direct imaging of human Rad51 nucleoprotein dynamics on individual DNA molecules. Proc. Natl. Acad. Sci. USA *106*, 361–368.

Hockemeyer, D., Sfeir, A.J., Shay, J.W., Wright, W.E., and de Lange, T. (2005). POT1 protects telomeres from a transient DNA damage response and determines how human chromosomes end. EMBO J. *24*, 2667–2678.

Hockemeyer, D., Daniels, J.P., Takai, H., and de Lange, T. (2006). Recent expansion of the telomeric complex in rodents: Two distinct POT1 proteins protect mouse telomeres. Cell *126*, 63–77.

Hwang, H., Buncher, N., Opresko, P.L., and Myong, S. (2012). POT1-TPP1 regulates telomeric overhang structural dynamics. Structure *20*, 1872–1880.

Jain, A., Liu, R., Ramani, B., Arauz, E., Ishitsuka, Y., Ragunathan, K., Park, J., Chen, J., Xiang, Y.K., and Ha, T. (2011). Probing cellular protein complexes using single-molecule pull-down. Nature *473*, 484–488.

Karlseder, J., Broccoli, D., Dai, Y., Hardy, S., and de Lange, T. (1999). p53- and ATM-dependent apoptosis induced by telomeres lacking TRF2. Science *283*, 1321–1325.

Kim, N.W., Piatyszek, M.A., Prowse, K.R., Harley, C.B., West, M.D., Ho, P.L., Coviello, G.M., Wright, W.E., Weinrich, S.L., and Shay, J.W. (1994). Specific association of human telomerase activity with immortal cells and cancer. Science *266*, 2011–2015.

Lane, A.N., Chaires, J.B., Gray, R.D., and Trent, J.O. (2008). Stability and kinetics of G-quadruplex structures. Nucleic Acids Res. *36*, 5482–5515.

Latrick, C.M., and Cech, T.R. (2010). POT1-TPP1 enhances telomerase processivity by slowing primer dissociation and aiding translocation. EMBO J. *29*, 924–933.

Lei, M., Podell, E.R., and Cech, T.R. (2004). Structure of human POT1 bound to telomeric single-stranded DNA provides a model for chromosome end-protection. Nat. Struct. Mol. Biol. *11*, 1223–1229.

Lei, M., Zaug, A.J., Podell, E.R., and Cech, T.R. (2005). Switching human telomerase on and off with hPOT1 protein in vitro. J. Biol. Chem. *280*, 20449–20456.

Lingner, J., Cooper, J.P., and Cech, T.R. (1995). Telomerase and DNA end replication: No longer a lagging strand problem? Science *269*, 1533–1534.

Liu, J.Q., Chen, C.Y., Xue, Y., Hao, Y.H., and Tan, Z. (2010). G-quadruplex hinders translocation of BLM helicase on DNA: A real-time fluorescence spectroscopic unwinding study and comparison with duplex substrates. J. Am. Chem. Soc. *132*, 10521–10527.

Lundblad, V., and Blackburn, E.H. (1993). An alternative pathway for yeast telomere maintenance rescues est1- senescence. Cell *73*, 347–360.

Makarov, V.L., Hirose, Y., and Langmore, J.P. (1997). Long G tails at both ends of human chromosomes suggest a C strand degradation mechanism for telomere shortening. Cell *88*, 657–666.

McElligott, R., and Wellinger, R.J. (1997). The terminal DNA structure of mammalian chromosomes. EMBO J. *16*, 3705–3714.

Mendez-Bermudez, A., Hidalgo-Bravo, A., Cotton, V.E., Gravani, A., Jeyapalan, J.N., and Royle, N.J. (2012). The roles of WRN and BLM RecQ helicases in the alternative lengthening of telomeres. Nucleic Acids Res. *40*, 10809–10820.

Mohaghegh, P., Karow, J.K., Brosh, R.M., Jr., Bohr, V.A., and Hickson, I.D. (2001). The Bloom's and Werner's syndrome proteins are DNA structure-specific helicases. Nucleic Acids Res. *29*, 2843–2849.

Murphy, M.C., Rasnik, I., Cheng, W., Lohman, T.M., and Ha, T. (2004). Probing single-stranded DNA conformational flexibility using fluorescence spectroscopy. Biophys. J. *86*, 2530–2537.

Oganesian, L., and Karlseder, J. (2011). Mammalian 5′ C-rich telomeric overhangs are a mark of recombination-dependent telomere maintenance. Mol. Cell *42*, 224–236.

Opresko, P.L., Sowd, G., and Wang, H. (2009). The Werner syndrome helicase/exonuclease processes mobile D-loops through branch migration and degradation. PLoS ONE *4*, e4825.

Paeschke, K., Capra, J.A., and Zakian, V.A. (2011). DNA replication through G-quadruplex motifs is promoted by the Saccharomyces cerevisiae Pif1 DNA helicase. Cell *145*, 678–691.

Paeschke, K., Bochman, M.L., Garcia, P.D., Cejka, P., Friedman, K.L., Kowalczykowski, S.C., and Zakian, V.A. (2013). Pif1 family helicases suppress genome instability at G-quadruplex motifs. Nature *497*, 458–462.

Palm, W., and de Lange, T. (2008). How shelterin protects mammalian telomeres. Annu. Rev. Genet. *42*, 301–334.

Palm, W., Hockemeyer, D., Kibe, T., and de Lange, T. (2009). Functional dissection of human and mouse POT1 proteins. Mol. Cell. Biol. *29*, 471–482.

Petraccone, L., Spink, C., Trent, J.O., Garbett, N.C., Mekmaysy, C.S., Giancola, C., and Chaires, J.B. (2011). Structure and stability of higher-order human telomeric quadruplexes. J. Am. Chem. Soc. *133*, 20951–20961.

Phatak, P., Cookson, J.C., Dai, F., Smith, V., Gartenhaus, R.B., Stevens, M.F., and Burger, A.M. (2007). Telomere uncapping by the G-quadruplex ligand RHPS4 inhibits clonogenic tumour cell growth in vitro and in vivo consistent with a cancer stem cell targeting mechanism. Br. J. Cancer *96*, 1223–1233.

Salazar, M., Thompson, B.D., Kerwin, S.M., and Hurley, L.H. (1996). Thermally induced DNA·RNA hybrid to G-quadruplex transitions: Possible implications for telomere synthesis by telomerase. Biochemistry *35*, 16110–16115.

Sfeir, A., Kosiyatrakul, S.T., Hockemeyer, D., MacRae, S.L., Karlseder, J., Schildkraut, C.L., and de Lange, T. (2009). Mammalian telomeres resemble fragile sites and require TRF1 for efficient replication. Cell *138*, 90–103.

Shakirov, E.V., Surovtseva, Y.V., Osbun, N., and Shippen, D.E. (2005). The Arabidopsis Pot1 and Pot2 proteins function in telomere length homeostasis and chromosome end protection. Mol. Cell. Biol. *25*, 7725–7733.

Shampay, J., Szostak, J.W., and Blackburn, E.H. (1984). DNA sequences of telomeres maintained in yeast. Nature *310*, 154–157.

Shay, J.W., and Bacchetti, S. (1997). A survey of telomerase activity in human cancer. Eur. J. Cancer *33*, 787–791.

Shay, J.W., and Wright, W.E. (2002). Telomerase: A target for cancer therapeutics. Cancer Cell *2*, 257–265.

Shin, D.S., Pellegrini, L., Daniels, D.S., Yelent, B., Craig, L., Bates, D., Yu, D.S., Shivji, M.K., Hitomi, C., Arvai, A.S., et al. (2003). Full-length archaeal Rad51 structure and mutants: Mechanisms for RAD51 assembly and control by BRCA2. EMBO J. *22*, 4566–4576.

Sigurdsson, S., Trujillo, K., Song, B., Stratton, S., and Sung, P. (2001). Basis for avid homologous DNA strand exchange by human Rad51 and RPA. J. Biol. Chem. *276*, 8798–8806.

Smogorzewska, A., and de Lange, T. (2002). Different telomere damage signaling pathways in human and mouse cells. EMBO J. *21*, 4338–4348.

Stavropoulos, D.J., Bradshaw, P.S., Li, X., Pasic, I., Truong, K., Ikura, M., Ungrin, M., and Meyn, M.S. (2002). The Bloom syndrome helicase BLM interacts with TRF2 in ALT cells and promotes telomeric DNA synthesis. Hum. Mol. Genet. *11*, 3135–3144.

Tahara, H., Shin-Ya, K., Seimiya, H., Yamada, H., Tsuruo, T., and Ide, T. (2006). G-Quadruplex stabilization by telomestatin induces TRF2 protein dissociation from telomeres and anaphase bridge formation accompanied by loss of the 3′ telomeric overhang in cancer cells. Oncogene *25*, 1955–1966.

Takai, K.K., Kibe, T., Donigian, J.R., Frescas, D., and de Lange, T. (2011). Telomere protection by TPP1/POT1 requires tethering to TIN2. Mol. Cell *44*, 647–659.

Tang, J., Kan, Z.Y., Yao, Y., Wang, Q., Hao, Y.H., and Tan, Z. (2008). G-quadruplex preferentially forms at the very 3′ end of vertebrate telomeric DNA. Nucleic Acids Res. *36*, 1200–1208.

Tárkányi, I., and Aradi, J. (2008). Pharmacological intervention strategies for affecting telomerase activity: Future prospects to treat cancer and degenerative disease. Biochimie *90*, 156–172.

Tarsounas, M., Muñoz, P., Claas, A., Smiraldo, P.G., Pittman, D.L., Blasco, M.A., and West, S.C. (2004). Telomere maintenance requires the RAD51D recombination/repair protein. Cell *117*, 337–347.

van Mameren, J., Modesti, M., Kanaar, R., Wyman, C., Peterman, E.J., and Wuite, G.J. (2009). Counting RAD51 proteins disassembling from nucleoprotein filaments under tension. Nature *457*, 745–748.

Vannier, J.B., Pavicic-Kaltenbrunner, V., Petalcorin, M.I., Ding, H., and Boulton, S.J. (2012). RTEL1 dismantles T loops and counteracts telomeric G4-DNA to maintain telomere integrity. Cell *149*, 795–806.

Varley, H., Pickett, H.A., Foxon, J.L., Reddel, R.R., and Royle, N.J. (2002). Molecular characterization of inter-telomere and intra-telomere mutations in human ALT cells. Nat. Genet. *30*, 301–305.

Vorlíčková, M., Chládková, J., Kejnovská, I., Fialová, M., and Kypr, J. (2005). Guanine tetraplex topology of human telomere DNA is governed by the number of (TTAGGG) repeats. Nucleic Acids Res. *33*, 5851–5860.

Wang, H., Nora, G.J., Ghodke, H., and Opresko, P. (2010). Single molecule studies of physiologically relevant telomeric tails reveals Pot1 mechanism for promoting G-quadruplex unfolding. J. Biol. Chem. *286*, 7479–7489.

Wang, Q., Liu, J.Q., Chen, Z., Zheng, K.W., Chen, C.Y., Hao, Y.H., and Tan, Z. (2011). G-quadruplex formation at the 3′ end of telomere DNA inhibits its extension by telomerase, polymerase and unwinding by helicase. Nucleic Acids Res. *39*, 6229–6237.

Watson, J.D. (1972). Origin of concatemeric T7 DNA. Nat. New Biol. *239*, 197–201.

Weinrich, S.L., Pruzan, R., Ma, L., Ouellette, M., Tesmer, V.M., Holt, S.E., Bodnar, A.G., Lichtsteiner, S., Kim, N.W., Trager, J.B., et al. (1997). Reconstitution of human telomerase with the template RNA component hTR and the catalytic protein subunit hTRT. Nat. Genet. *17*, 498–502.

Wong, A., and Wu, G. (2003). Selective binding of monovalent cations to the stacking G-quartet structure formed by guanosine 5′-monophosphate: A solid-state NMR study. J. Am. Chem. Soc. *125*, 13895–13905.

Wright, W.E., Tesmer, V.M., Huffman, K.E., Levene, S.D., and Shay, J.W. (1997). Normal human chromosomes have long G-rich telomeric overhangs at one end. Genes Dev. *11*, 2801–2809.

Wu, L., Multani, A.S., He, H., Cosme-Blanco, W., Deng, Y., Deng, J.M., Bachilo, O., Pathak, S., Tahara, H., Bailey, S.M., et al. (2006). Pot1 deficiency initiates DNA damage checkpoint activation and aberrant homologous recombination at telomeres. Cell *126*, 49–62.

 

Ye, J.Z., Hockemeyer, D., Krutchinsky, A.N., Loayza, D., Hooper, S.M., Chait, B.T., and de Lange, T. (2004). POT1-interacting protein PIP1: A telomere length regulator that recruits POT1 to the TIN2/TRF1 complex. Genes Dev. *18*, 1649–1654.

Yu, H.Q., Miyoshi, D., and Sugimoto, N. (2006). Characterization of structure and stability of long telomeric DNA G-quadruplexes. J. Am. Chem. Soc. *128*, 15461–15468.

Zahler, A.M., Williamson, J.R., Cech, T.R., and Prescott, D.M. (1991). Inhibition of telomerase by G-quartet DNA structures. Nature *350*, 718–720.

Zaug, A.J., Podell, E.R., and Cech, T.R. (2005). Human POT1 disrupts telomeric G-quadruplexes allowing telomerase extension in vitro. Proc. Natl. Acad. Sci. USA *102*, 10864–10869.

Zaug, A.J., Podell, E.R., Nandakumar, J., and Cech, T.R. (2010). Functional interaction between telomere protein TPP1 and telomerase. Genes Dev. *24*, 613–622.

Zhang, Y., Chen, L.Y., Han, X., Xie, W., Kim, H., Yang, D., Liu, D., and Songyang, Z. (2013). Phosphorylation of TPP1 regulates cell cycle-dependent telomerase recruitment. Proc. Natl. Acad. Sci. USA *110*, 5457–5462.